Investigating the role of irradiation defects during UO_2 oxidative dissolution

R. Mohun[a*], L. Desgranges[a], A. Canizarès[b], N. Raimboux[b], F. Duval[b1], R. Omnee[b], C. Jégou[c], S. Miro[c] & P. Simon[b]

[a.] *CEA, DEN, DEC, SESC, F-13108 Saint-Paul-lez-Durance, France*
[b.] *CNRS, UPR 3079 CEMHTI, et Université d'Orléans, 45071 Orléans, France*
[c.] *CEA, DEN, DTCD, F-30207 Bagnols sur Cèze, France*

Abstract

In this study, the behavior of alpha irradiation-induced defects in UO_2, when exposed to different interfaces, is investigated. Raman spectroscopy is used to measure the formation kinetics of irradiation defects in UO_2 leached under oxidizing water environment and the data are then compared to a reference UO_2/Ar system. The results reveal that the presence of either aerated water or inert argon gas modifies the formation kinetics of irradiation defects. The UO_2 alteration in aerated water leads to the precipitation of secondary phases in the form of studtite and water chemical analysis reveals that the UO_2 dissolution mechanism proceeds without the formation of an oxidized UO_2 layer.

Keywords: Irradiation defects, Raman spectroscopy, aerated water, secondary phases

1. Introduction

The safe management of spent nuclear fuels remains one of the main concerns facing the modern nuclear industry and a major international effort is currently underway in order to propose suitable management and disposal procedures. One major scientific question associated with this industrial issue deals with the behavior of spent nuclear fuels in the presence of water. It is of utmost importance to acquire sufficient data for understanding the irradiated fuel leaching behavior.

The anoxic dissolution of nuclear fuels has been extensively studied and suitable mechanisms have been proposed by Shoesmith *et al.* [1]. Relevant data on the oxidative dissolution of UO_2 and MOX fuels under the influence of irradiation are also available [2, 3, 4, 5, 6]. It is worth noting that previous studies were principally devoted to characterizing the oxidation of the fuel matrix [7], the uranium and plutonium release rates [8, 9], and the effect of H_2O_2 and radiolytic radicals on the dissolution mechanisms [10, 11, 12, 13]. The effect of burn-up has also been reported through the measurements of fission product release [14, 15, 16]. However, little is known about the irradiation defects within the spent nuclear fuels during their interaction with the aqueous medium.

Post-irradiation, about 95% of the spent fuel still consists of UO_2 while the remaining 5% is distributed amongst fission products and transuranic elements. The dissolution of the UO_2 matrix

[1] now at ISTO, CNRS/Université Orleans, F-45100 Orleans.

thus governs the release of radionuclides from the irradiated fuels. It has been speculated that irradiation-induced damages involving the accumulation of point defects in the crystalline structure affect the chemical durability of nuclear fuels [17, 18]. However, the latter is difficult to quantify in UO_2 because several factors impact its normal dissolution such as the oxidation of U(IV) into more soluble U(VI), amongst others [19].

Several studies have been performed using CeO_2 compounds that aimed to investigate the specific role of defect structures. Oxygen vacancy defects can be induced in CeO_2 by doping, high-temperature annealing in an oxygen-deficient atmosphere or even ionic irradiation. Findings from previous studies have shown that the cationic release rate of CeO_{2-x} is more significant compared to stoichiometric CeO_2 compounds. For instance, Horlait *et al.* [20] evidenced a considerable decrease in the chemical durability of CeO_2 doped with Ln ions. Similar leaching trends were also observed for CeO_{2-x} obtained through both precise synthesis methods [19] and Xe ionic implantation [21]. On the other hand, the amorphization of ceramic wastes also leads to a significant effect on the leaching mechanisms as previously reported by Ollila e*t al.* [22] and Matzke [23]. Though UO_2 does not undergo such behavior during ionic implantation, the presence of irradiation-induced lattice defects might influence the dissolution rate.

This study aims to elucidate the effect of alpha irradiation on the UO_2 oxidative dissolution mechanisms and also provides a rigorous analysis of the irradiation defects during a potential UO_2 matrix-water interaction by means of Raman spectroscopy. The latter is a powerful characterization tool for the identification of the altered secondary phases formed during dissolution experiments [24]. Raman spectroscopy has also proven its reliability for the investigation of atomic defects in nuclear fuels. The occurrence of a specific Raman signature, referred to as the Raman triplet defect bands, in both doped and irradiated UO_2, appears as a promising path for the understanding of atomic defects in nuclear fuels [25, 26, 27, 28]. In this paper, we present the application of a newly developed *in situ* experimental setup to monitor the formation kinetics of the Raman defect bands during the alpha irradiation of UO_2 when exposed to different interfaces.

2. Experimental

2.1. Materials

Sintered UO_2 ceramics (8 mm diameter and 300 µm thickness) were manufactured at the Laboratoire des Combustibles Uranium (LCU) at CEA-Cadarache, France. The pellets were heat-treated at 1400°C under dry Ar/H_2 and mirror polished on one surface for subsequent *in situ* and *ex situ* characterizations.

2.2. Irradiation conditions

The alpha irradiation was performed using a cyclotron device at the “Conditions Extrêmes et Matériaux: Haute Température & Irradiation” (CEMHTI) Laboratory at Orléans, France. The

irradiation was carried out under two different settings: *(a)* UO_2 in contact with a reactive interface (aerated water) and *(b)* UO_2 in the presence of an inert gaseous medium (argon gas).

For both experiments, the UO_2 pellets were irradiated with a 45 MeV alpha beam during 2 hours to deliver a final fluence of 7.07 x 10^{15} α/cm^2. Under such conditions, the alpha particles are allowed to pass through the pellets and are then attenuated in the contact medium. An estimated defect concentration of 3.62 x 10^{-2} in the UO_2 bulk per ion was determined by the SRIM simulation software [29].

2.2.1. Irradiation of UO_2 in contact with aerated water

A full description of the experimental installation used in this study was previously detailed by our colleagues [30]. The setup consists of an irradiation chamber and a safety area. For the leaching experiment, a newly developed sample holder was placed in the irradiation chamber which maintained the mirror polished UO_2 surface in contact with aerated water and the non-polished surface was exposed to the alpha beam. Before irradiation, the pellet was washed with carbonated water (10^{-3} M) during two cycles of sequential pre-leaching (2 x 1 hr.) to remove any traces of oxidized layer from the UO_2 surface. Two other sequential pre-leaching with pure aerated demineralized water were also performed (2 x 1 hr.) to quantify the concentration of dissolved uranium before irradiation. The sample holder was then filled with 15 mL aerated deionized water and the pH was kept in equilibrium with air, close to ~5.5.

The alpha irradiation induces atomistic damages in the UO_2 bulk. The incident ions then emerge from the UO_2 disk at 5 MeV and are attenuated over a distance of 37 μm in the water solution [29]. The attenuation of the alpha particles initiates a water radiolysis process which leads to the production of several radiolytic species such as radicals, hydrated electrons and hydrogen peroxide (H_2O_2). During alpha water radiolysis, the formation of molecular species is favored mainly due to the recombination of short-lived radicals in the tracks since the density of ionization events is greater with alpha particles compared to low-LET particles [31, 32]. Though short-lived radicals can also contribute to the dissolution experiment, this study was solely focused on the effect of highly oxidizing H_2O_2. Long-lived H_2O_2 is more stable and diffuses homogeneously in the solution. Thus, their effect on the dissolution can be easily quantified and is discussed in this paper. A motorized Raman probe positioned on a three-dimensional XYZ motion–control system (Newport MFA 25 and ILS 250 stages) was installed in the irradiation chamber for the *in situ* monitoring of the UO_2/H_2O interface during irradiation.

The essential components of the *in situ* Raman spectroscopy were kept in the safety area, located 20 m away from the irradiation chamber, to prevent equipment damage due to irradiation. The safety area and the irradiation chamber were relayed by means of optical fibers and electric cables.

2.2.2. Irradiation of UO_2 under inert gaseous (Ar) medium

The UO_2 ceramic was placed in the same configuration as detailed in Section 2.2.1, except that the aerated water solution was replaced by a chemically inert gaseous medium. Argon gas was used for this study because it provides an inert UO_2 boundary to which the mechanisms occurring near the UO_2-H_2O interface can be compared. The attenuation of alpha particles in the gaseous medium generates an argon plasma which appears as an intense and narrow peak at 825 cm^{-1} on the Raman spectrum with the red (632.8 nm) excitation laser.

This experiment is similar to the study previously performed by Guimbretière *et al.* [33] except that the measurements were largely optimized to allow the acquisition of Raman spectra of the highest quality.

2.3. *In situ* Raman measurements

The irradiation-induced changes occurring near the UO_2 interface were monitored by a Renishaw RA-100 Raman Analyzer. The laser spot of the portable Renishaw RA-100 device is ~8 µm. Guimbrètiere *et al.* [26] showed the existence of a UO_2 grain boundary Raman signal at 555 cm^{-1}. For the need of this study, a UO_2 disk was carefully chosen which did not show significant contribution of the grain boundary signal because the latter appears in the same spectral range as the irradiation-induced Raman signals.

A 632.8 nm He-Ne red laser and a holographic grating of 1800 grooves/mm were sufficient to allow 2-3 cm^{-1} spectral resolution. The spectroscopy uses a Mitutoyo microscope objective (x20) which enables a focal length of 30.5 mm, giving a depth field of about 300 µm. However, the high absorbing properties of UO_2 restrict the probing depth only to the pellet surface. The Raman spectra were obtained with an acquisition time of 120s after 5 accumulations in the 300-1000 cm^{-1} spectral range using a multichannel CCD (576 x 401 pixels) detector.

2.4. *Ex situ* Raman characterizations

The *ex situ* measurements of the irradiated UO_2 disks were carried out by a Renishaw Invia Reflex high-confocal spectrometer. The latter was also equipped with a 632.8 nm excitation laser and a holographic grating of 1800 grooves/mm for a spectral acquisition between 300 and 900 cm^{-1}. The UO_2 grains and grain boundary attacks were analyzed by performing Raman spectral mappings over a selected area of the leached surface after the dissolution experiment. The dimensions of the chosen area were 55 x 25 μm^2 on the x and y-axis respectively, with a moving step of 1 µm in the snake mapping mode.

2.5. Scanning Electron Microscopy (SEM) and X-ray diffraction (XRD) measurements

The SEM and XRD measurements were carried out at the LCU lab at CEA-Cadarache. For the SEM analysis, a Philips XL30 FEG device was used and part of the UO_2 leached surface was

covered with a thin silver lac film to increase electron conduction for the acquisition of high-resolution images.

In regard to XRD measurements, a D8 Bruker diffractometer (45 kV, 40 mA) mounted in a Bragg–Brentano configuration with copper radiation from a conventional tube source ($\lambda K\alpha_1$ = 1.5406 Å, $\lambda K\alpha_2$ = 1.5444 Å) was used. The diffractometer is equipped with a graphite monochromator and a NaI scintillation 269 detector. The diffraction patterns were recorded for a scan in the 20°-140° (2θ) range using a 0.01° step with a counting step of 5s. The total measuring time was 16 hrs.

2.6. Irradiated water solution analysis

The water solution was removed from the sample holder and transferred into suitable flasks after the irradiation experiment. The solution analysis was performed at the Laboratoire des Matériaux et Procédés Actifs (LMPA) at CEA-Marcoule to determine the concentration of radiolytic H_2O_2 and dissolved uranium.

Molecular H_2O_2 rapidly dissociates into hydroxyl radicals under continuous UV light exposure. The flasks were thus wrapped in aluminum foil and stored at low temperature (~4°C) to measure the quantitative amount of radiolytic H_2O_2 produced by the alpha particles. The spectrophotometric Ghormley method [34] was used to determine the concentration of H_2O_2 in the solution ranging from 4×10^{-6} M to 2×10^{-4} M. The dissolved uranium in the solution was measured by a laser-induced Kinetic Phosphorescence Analyzer (KPA) with a quantitative limit of 0.1 µg/L.

3. Results

3.1. *In situ* Raman measurements

Figure 1 shows the *in situ* Raman spectra acquired during the alpha irradiation of the UO_2/H_2O interface.

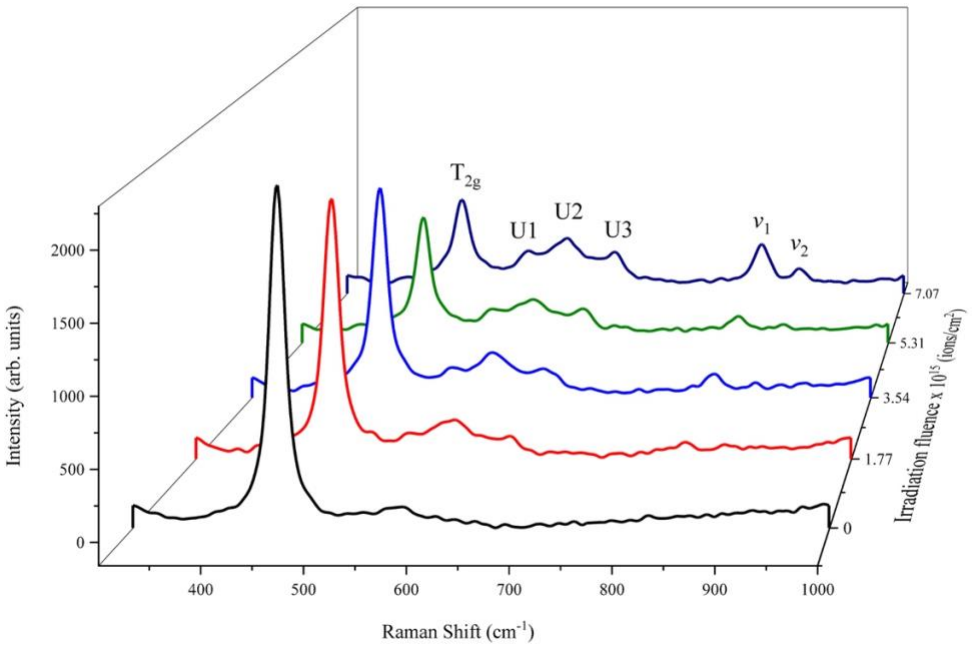


Figure 1: *In situ* Raman acquisitions of the UO_2/H_2O system as a function of increasing alpha irradiation fluence

Before irradiation, the Raman spectrum of the UO_2 sample indicates the presence of the triply degenerate Raman active T_{2g} mode occurring at 445 cm^{-1}. This peak is referred to as the symmetry Raman-allowed phonon scattering of UO_2 and is the signature of compounds sharing the Fm3m space group. The absence of other noticeable peaks suggests that the UO_2 disk was close to stoichiometry before the irradiation experiment.

The alpha irradiation affects the T_{2g} peak (decrease in the intensity accompanied by a peak broadening). Similar observations were previously reported by Guimbretière *et al.* [35]. The irradiation also induces the apparition of three additional peaks in the 500-660 cm^{-1} spectral range. These peaks are referred to as the Raman triplet defect bands (U1: ~527 cm^{-1}, U2: ~575 cm^{-1} & U3: ~635 cm^{-1}) and correspond to the presence of irradiation damages [36, 37, 38, 39]. Figure 1 shows that the intensity of the defect bands grows continuously with the increase of the alpha irradiation fluence and is consistent with the increase defect concentration in the UO_2 bulk.

Radiolytic H_2O_2 can enhance both the UO_2 oxidation and the uranium dissolution rate in the form of uranyl ions (UO_2^{2+}). These ions precipitate as secondary phases on the pellet surface once the water solution reaches the solubility limit for the formation of U(VI) phases. The two distinct peaks occurring at 820 cm^{-1} and 865 cm^{-1} on the spectra are signatures of the studtite secondary phase ($UO_2.(O_2).4H_2O$). According to Amme *et al.* [24], the 820 cm^{-1} peak corresponds to the symmetrical axial stretching mode of uranyl ion (UO_2^{2+}) (ν_1) and the 865 cm^{-1} band is attributed to peroxide ion (O_2^{2-}) (ν_2) in the studtite structure.

3.2. SEM analysis

Prior to irradiation, the SEM image of the polished surface clearly indicates the UO_2 grains and grain boundaries (Figure 2a). At the end of the leaching experiment, the irradiated UO_2 disk was dismantled from the sample holder and dried to analyze the surface microscopic evolution.

The radiolytic attack brings significant changes to the microstructure. Figure 2b shows the formation of a homogeneously distributed thick altered layer displaying micro-cracks over the entire surface. The sample was tilted to 35° to the direction of the electron beam and the thickness of the altered layer was estimated to be in the 1-2.5 µm range (Figure 2c & Figure 2d).

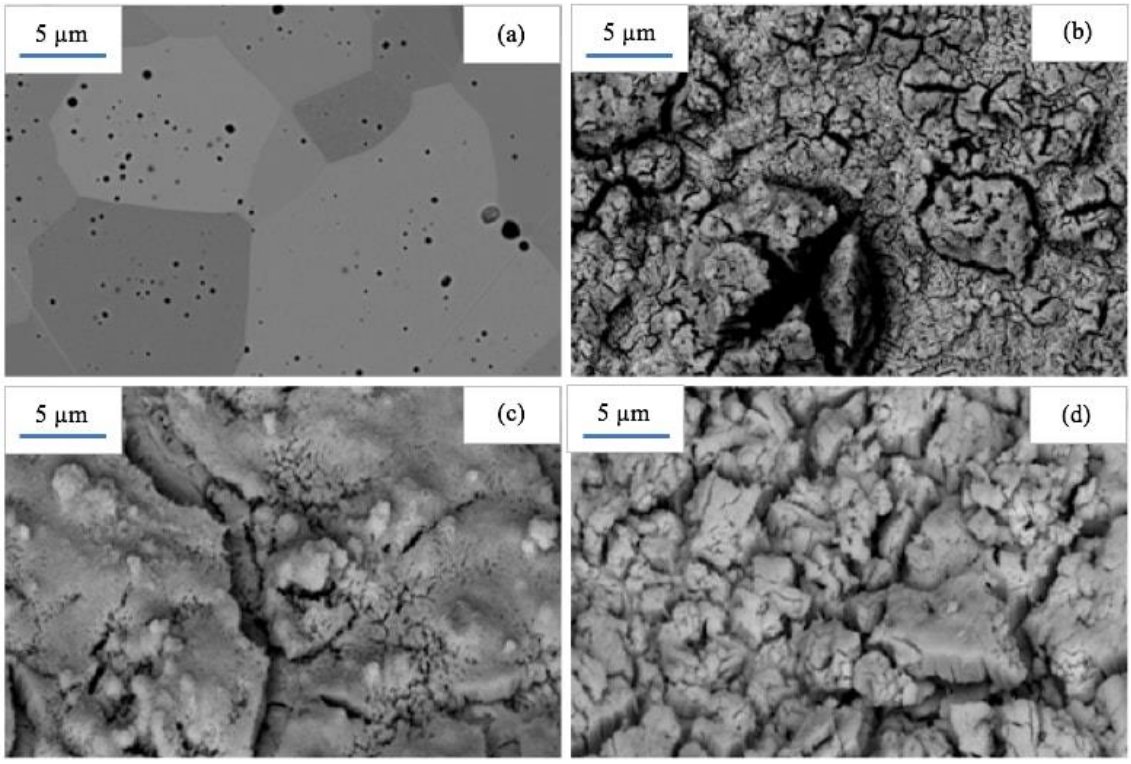


Figure 2: SEM images of the UO_2 surface *(a)* before and *(b-d)* after leaching under alpha irradiation; *(b)*: tilt 0° & *(c-d)*: tilt 35°

3.3. *Ex situ* Raman mapping

The SEM images show that the studtite phase remains thin enough to be transparent in the visible spectral range. The *ex situ* Raman mapping was performed to extract relevant information regarding the UO_2 grains, grain boundaries and studtite phase.

Figure 3 shows the microscope image of the mapped leached surface area. The bright green color indicates the highly oxidized regions and the blue color corresponds to the low altered zones. The high intensity of the studtite phase shows that the grain boundary regions were preferentially

attacked compared to the UO_2 grains. These observations are in good agreement with Traboulsi *et al.* [40].

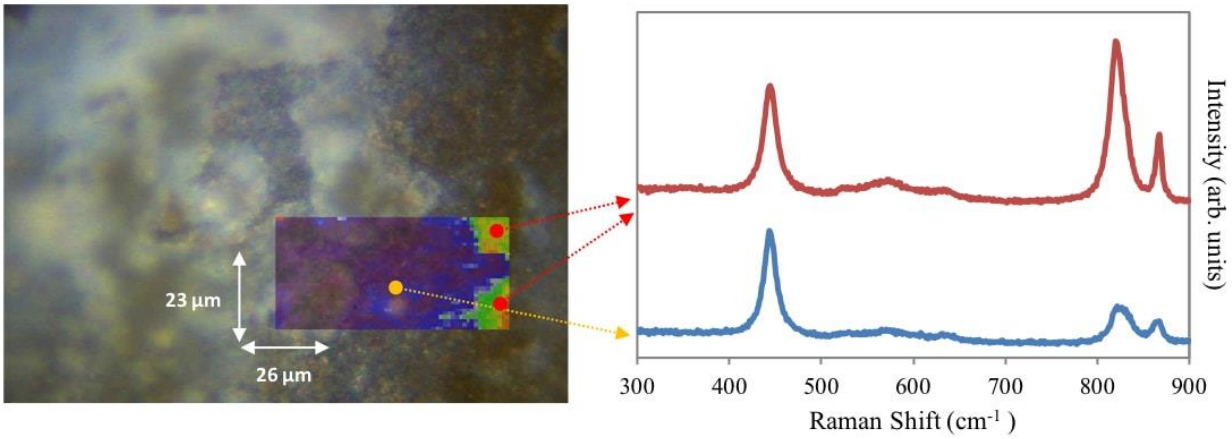


Figure 3: Space-resolved Raman spectral mapping of the irradiated UO_2 surface showing the grains (Blue color) and grain boundary regions (Green color). (For interpretations of the references to color in this figure, the reader is referred to the online version of this manuscript).

3.4. XRD measurements

XRD method was used to confirm the exact nature of the secondary altered phases. The obtained data (not presented in this paper) showed the presence of metastudtite ($UO_2(O_2).2H_2O$) on the fuel surface. The presence of metastudtite evidenced at this stage of analysis was due to the combined effects of air exposure and studtite dehydration after the SEM and *ex situ* Raman analysis [41]. The XRD measurements thus suggest that studtite was initially precipitated during the leaching experiment and are therefore consistent with the *in situ* and *ex situ* Raman data. It is worth noting that the schoepite phase ($UO_3.2H_2O$) was not unambiguously observed in our study [24].

3.5. Solution analysis

The dissolved uranium concentration before irradiation was measured from the water solution used for the two sequential pre-leaching steps. The uranium release was observed to decrease from 1.93 ± 0.20 µg/L to 0.121 ± 0.012 µg/L.

The concentration of radiolytic H_2O_2 and dissolved uranium contained in the solution after irradiation were quantified and are presented in Table 1. The analysis also revealed a high concentration of fluoride and chloride ions in the water solution. These ions originate from the polychlorotrifluoroethylene (PCTFE) polymer used for the fabrication of the sample holder. The polymer material was chosen because it provides excellent resistance to radiolytic attack. The

complexing and corrosive characteristics of fluoride ions are likely to affect the UO_2 dissolution mechanisms.

Table 1: Detailed analysis of the irradiated solution showing the concentration of radiolytic H_2O_2 and dissolved uranium. The concentration of fluoride and chloride ions released from the sample holder is also reported

	Molecular H_2O_2 (mol/L)	**Dissolved uranium (µg/L)**	**Fluoride ions (µg/L)**	**Chloride ions (µg/L)**
Measured value	5.4×10^{-3}	207	890	570
Uncertainty	$\pm 1.1 \times 10^{-3}$	± 21	± 180	± 110

4. Discussion

The UO_2 oxidative dissolution mechanisms will first be discussed based on the findings obtained during the detailed chemical analysis of the irradiated water solution. The formation kinetics of alpha irradiation-induced defects in the UO_2 bulk will then be analyzed to determine their behavior during the dissolution process.

4.1. UO_2 oxidative dissolution

The measured H_2O_2 concentration is found to be of the same order as those previously reported by Corbel *et al.* [2] and Sattonnay *et al.* [4]. Shoesmith *et al.* [42] investigated the effect of H_2O_2 on the UO_2 dissolution rate. The authors showed that the concentration of dissolved uranium increases with a first-order dependence when the H_2O_2 concentration is close to 5.4×10^{-3} mol/L. The saturation index (SI) of the irradiated water solution for the studtite precipitation was then determined using the equilibrium reaction between UO_2^{2+} ions and H_2O_2 (Equation 1).

$$UO_2{}^{2+}{}_{(aq)} + H_2O_2{}_{(aq)} + 4H_2O_{(aq)} \leftrightarrow UO_2(O_2).4H_2O_{(s)} + 2H^+{}_{(aq)} \quad (1)$$

The SI for the precipitation of studtite phase is obtained from Equation 2.

$$SI_{(studtite)} = log \frac{[UO_2{}^{2+}].[H_2O_2]}{[H^+]^2} \quad (2)$$
$$Ks_{studtite}$$

Where $\log Ks_{Studtite} = -2.86$ and represents the solubility constant for studtite [43].

The conditions for studtite precipitation are as follows:

SI < 0: under-saturation (no precipitation of secondary phases)
SI ≥ 0: solubility limit for the formation of studtite (precipitation of secondary phases is favored)

The calculated saturation index value (SI = 3.53) indicates that the irradiated water solution was over-saturated and the formation of the studtite phase was favored. This result is in good agreement with the Raman, SEM, and XRD findings. According to Equation 1, the precipitation of secondary phases increases the solution acidity. In this study, it was evidenced that the pH of the water solution decreased from ~5.5 (before irradiation) to 4.5 (after irradiation). According to Torrero *et al.* [44], the UO_2 oxidative dissolution mechanisms proceed with little surface oxidation under such slightly acidic conditions.

The high concentration of corrosive fluoride ions should also be considered in the dissolution mechanisms mainly due to their excellent complexing ability toward uranium ions. They form strong $UO_2F^+_{(aq)}$ ligands with free uranyl ions in the solution but also tend to complex the UO_2 surface. Thus, the combined effects of solution pH and complexing ions suggest that the dissolution mechanisms occur without the formation of an oxidized UO_2 layer. Raman measurements confirmed the absence of fuel oxidation because no peaks relevant to hyper-stoichiometric UO_2 were observed. Indeed, compared to irradiated UO_2 where the Raman defect bands (U1: ~527 cm^{-1}, U2: ~575 cm^{-1} & U3: ~635 cm^{-1}) appear in the 500-660 cm^{-1} spectral range, hyper-stoichiometric UO_2 is characterized by a small hump at 530 cm^{-1} and an intense asymmetric band at 630 cm^{-1} [45, 46, 47, 48, 49].

4.2. In situ Raman analysis: Irradiation defects

Figure 4 shows three *in situ* Raman spectra (only the 450-700 cm^{-1} range) of the UO_2/H_2O system irradiated at different alpha fluence. The figure depicts the growing intensity of the defect bands (U1, U2 & U3) under increasing irradiation fluence.

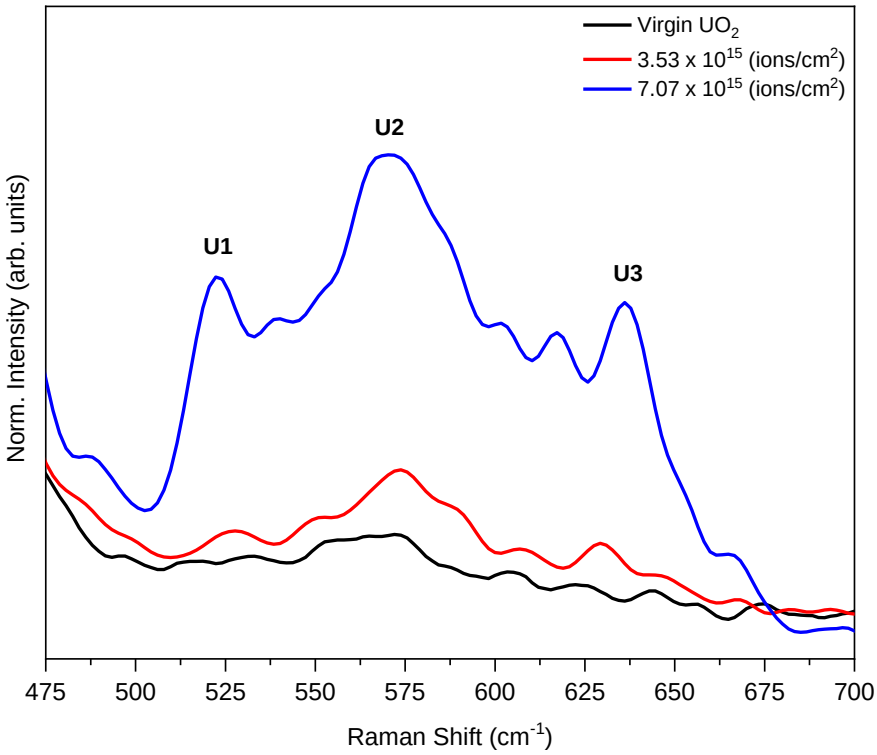


Figure 4: *In situ* evolution of the Raman triplet defect peaks during irradiation of the UO_2/H_2O system

The *in situ* spectra were collected with an excellent signal-to-noise ratio and offered the advantage of a precise analytical data treatment to study the kinetics of the U1, U2 & U3 bands. The defect kinetics, presented in Figure 5, were obtained after the removal of background noises (baseline subtraction) followed by averaging the intensity of the triplet defect bands occurring between 500 and 660 cm^{-1}.

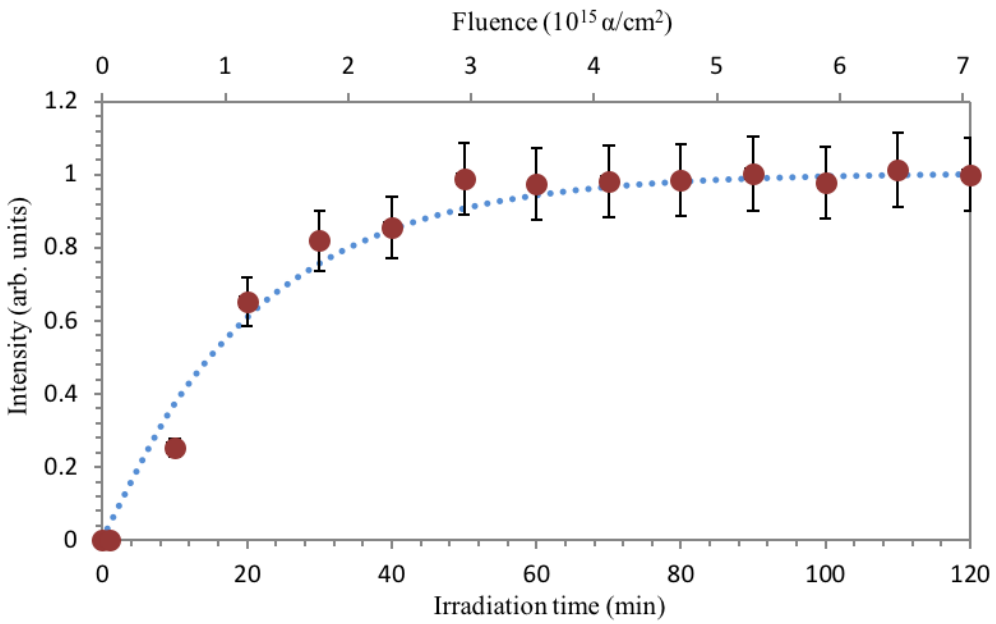


Figure 5: Kinetics of Raman triplet defect bands intensity (Red dots) fitted with the Direct Impact model (Blue dotted line) for the UO_2/H_2O system under alpha irradiation. (For interpretations of the references to color in this figure, the reader is referred to the online version of this manuscript).

The data presented in Figure 5 were then compared to the reference UO_2/Ar system to provide a better interpretation of the observed kinetics. Figure 6 illustrates the *in situ* Raman spectra acquired during the alpha irradiation of the UO_2 disk exposed to the chemically inert argon environment.

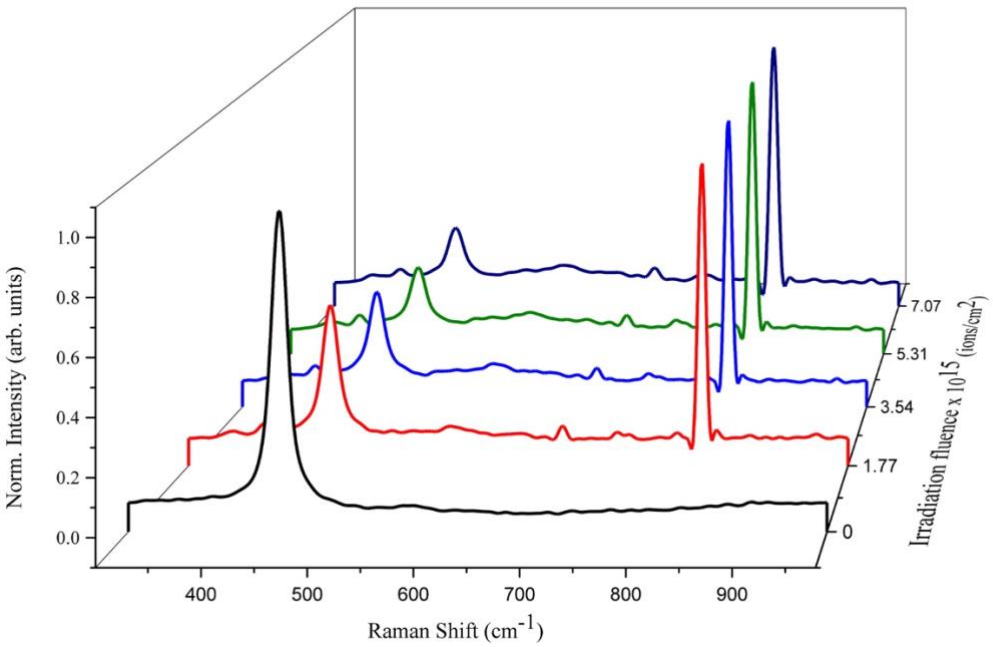


Figure 6: *In situ* evolution of the Raman spectra acquired during the alpha irradiation of the UO_2/Ar system

Figure 6 shows an important decrease of the T_{2g} intensity during the initial stages of irradiation. The T_{2g} band broadening as a function of irradiation fluence can also be evidenced. The argon plasma resulting from the attenuation of alpha particles in the gaseous contact medium appears as the intense peak at 825 cm^{-1} (relative to 633 nm reference, *i.e.*, 667.9 nm as wavelength). Another plasma line of lower intensity can be observed just below 700 cm^{-1}. The high intensity of the plasma rays slightly masks the Raman triplet defect bands and needs to be corrected to extract the defect kinetics.

Figure 7 highlights the 475-700 cm^{-1} spectral range and the behavior of the U1, U2 and U3 peaks during the irradiation of the UO_2/Ar system can be observed.

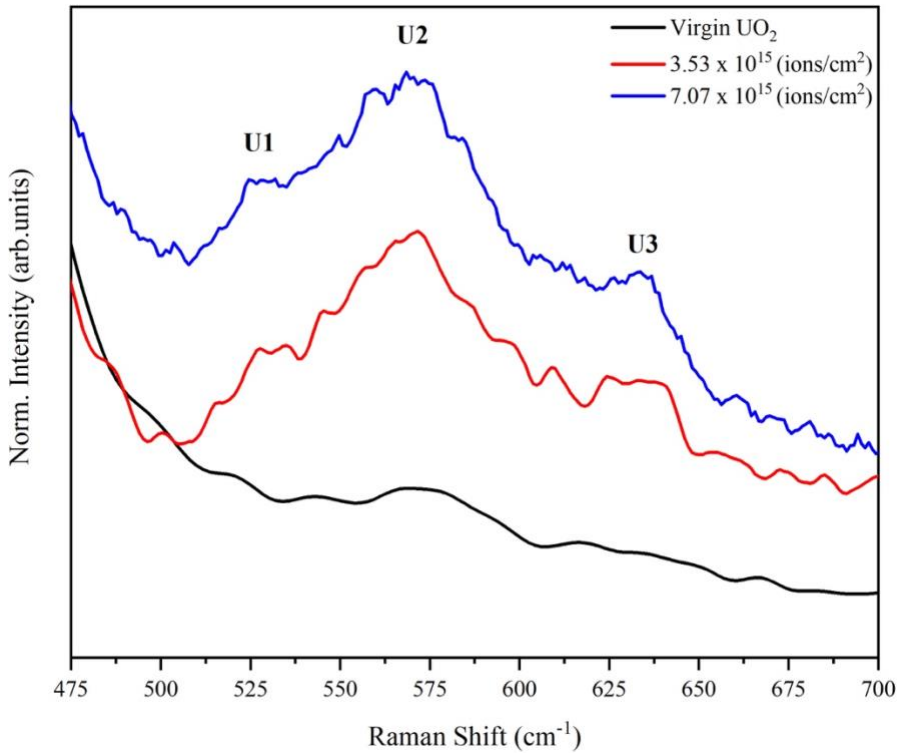


Figure 7: *In situ* evolution of the Raman triplet defect peaks during irradiation of the UO_2/Ar system

The kinetics of the defect bands were extracted using a similar data treatment as employed for the UO_2/H_2O system and are presented in Figure 8.

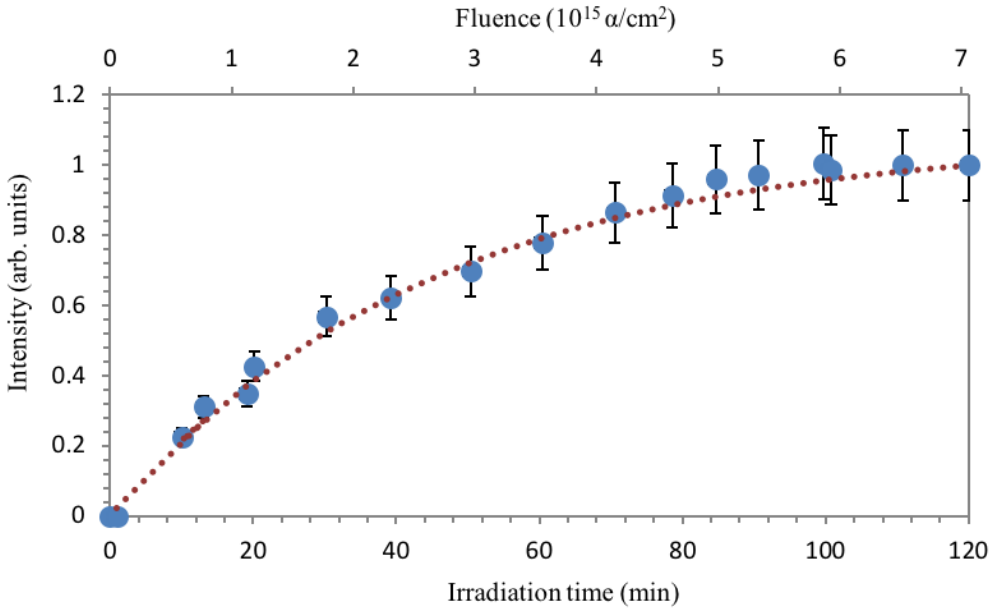


Figure 8: Kinetics of Raman defect bands intensity (Blue dots) fitted with the Direct Impact model (Red dotted line) for the UO_2/Ar system under alpha irradiation. (For interpretations of the references to color in this figure, the reader is referred to the online version of this manuscript).

The kinetics of the Raman triplet defect bands for both UO_2/H_2O and UO_2/Ar systems follow a unique kinetic; characterized by a rapid intensity increase during the initial stages of irradiation before reaching saturation. The initial increase of the defect bands intensity corresponds to the production of irradiation defects while the saturation phase indicates the elimination/annihilation step of the defects respectively. Guimbretière *et al.* [33] demonstrated that the two-staged kinetics can be fitted by a simple Direct Impact (DI) model which relates the defect concentration (ρD) and the alpha dose (Dα) (Equation 3).

$$d\rho_D/dD_\alpha = R_\alpha - B\rho_D \quad (3)$$

R_α is the number of irradiation defects (I.D) produced per unit of path length traveled by alpha particles (I.D/cm.α). (B x ρ_D) corresponds to the annihilation term describing the recombination of irradiation defects. The B-parameter defines the annealing rate constant (cm^2/α) and ρ_D is in I.D/cm^3. Equation 3 can also be expressed in the form of Equation 4.

$$\rho_D = \rho_{D(\infty)}\ x\ (1 - e^{-BD_\alpha}) \quad (4)$$

$\rho_{D(\infty)}$ is the defect concentration at saturation.

The theoretical exponential fits of the defect bands kinetics shown in Figure 5 & Figure 8 were important to set the numerical interpretations for $\rho_{D(\infty)}$ and the B-parameter. The obtained values are presented in Table 2.

Table 2: Comparison of the defect concentrations at saturation ($\rho_{D(\infty)}$) and the defect annealing parameter (B) for the UO_2/Ar and UO_2/H_2O systems

Scenario studied	$\rho_{D(\infty)}$	Annealing Parameter (B)
UO_2/Ar	1.10 ± 0.023	$3.75 \times 10^{-16} \pm 1.93 \times 10^{-17}$
UO_2/H_2O	1.02 ± 0.022	$7.95 \times 10^{-16} \pm 7.29 \times 10^{-17}$

Table 2 shows that the defect kinetics for the UO_2/Ar can be modeled with an annealing rate constant of $3.75 \times 10^{-16} \pm 1.93 \times 10^{-17}$ cm^2/α. This observation is in good agreement with the values reported by Guimbretière *et al.* [33] ($10^{-16} \pm 10^{-17}$ cm^2/α) and Weber [50] (0.85×10^{-16} cm^2/α). The slight variance can be attributed to different UO_2 samples density used in the mentioned studies. The fit for the UO_2/H_2O gives a B-parameter of $7.95 \times 10^{-16} \pm 7.29 \times 10^{-17}$ cm^2, *i.e.*, twice the value obtained for the reference UO_2/Ar. These findings suggest that the elimination of defects is accelerated when the irradiation experiment is carried out under a chemically reactive environment. This can be observed from Figure 9 which shows that the saturation stage for the UO_2/H_2O is attained much faster compared to the inert argon environment.

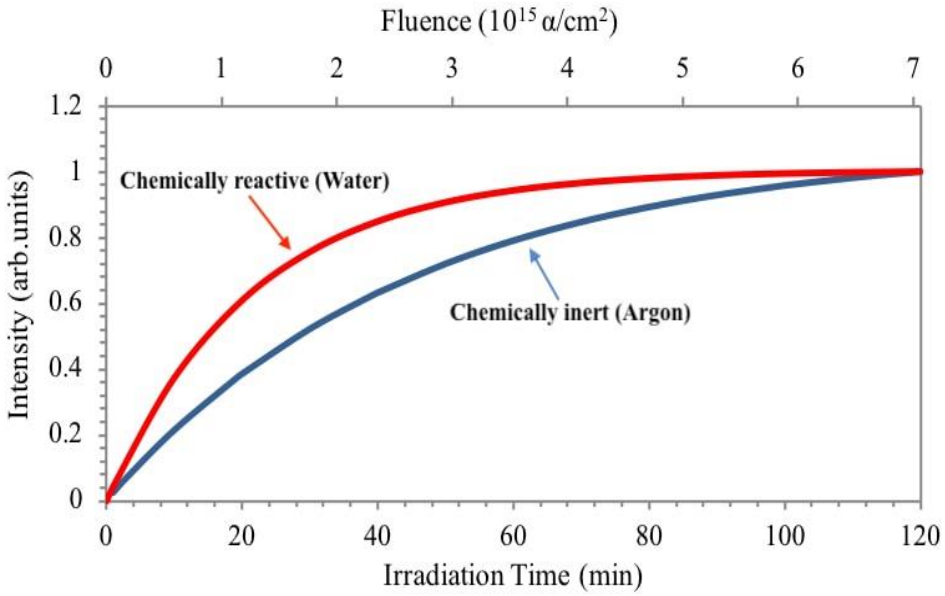


Figure 9: Comparison of the *in situ* irradiation defects kinetics of the UO_2/Ar (Blue color) and the UO_2/H_2O (Red color). (For interpretations of the references to color in this figure, the reader is referred to the online version of this manuscript).

The difference in the kinetics can be interpreted by considering the UO_2 boundary surface exposed to the contact medium during the alpha irradiation. For the UO_2 leaching experiment, chemical reactions are more likely to be involved near the UO_2-H_2O interface and contribute to the dissolution of the UO_2 disk. However, the increase in the defect annealing step observed during the leaching study gives indication to suggest that the alpha-induced irradiation defects may also be involved in these chemical reactions. In doing so, the UO_2 boundary layer acts as sinks and governs

the annealing of defects. Tocino *et al.* [51] and Corkhill *et al.* [19] recently highlighted the importance of atomistic defects during the dissolution of uranium mixed oxides and cerium compounds respectively. The authors showed that the high leaching rate was related to the reduced chemical durability of the materials due to the presence of crystal defects such as oxygen vacancies. These findings thus indicate that irradiation defects should also be considered in the chemical reactions occurring near the fuel matrix-water interface.

However, such chemical reactions do not hold much significance for the UO_2/Ar system due to the inert chemical characteristic of the argon gas. The elimination of irradiation defects solely depends on a simple vacancy-interstitial recombination mechanism. The defects annealing step is likely to be delayed as a sufficiently high defect concentration should first be reached in the UO_2 bulk.

It is worth noting that the *in situ* Raman analysis gives an overview regarding the behavior of irradiation damages under different interfaces but unfortunately does not allow us to identify the types of defects involved, *i.e.,* uranium/oxygen at interstitial/vacancy positions. To complete this study, further investigations are still required to provide additional information relevant to the Raman triplet defect bands.

5. Conclusions

In this study, a newly designed *in situ* Raman installation was employed to characterize the behavior of a UO_2 disk in contact with deionized aerated water under the influence of a 45 MeV alpha beam. The objective of this work was to measure the formation kinetics of irradiation defects and the obtained data were then compared to a reference UO_2/Ar system.

The irradiation defects for both UO_2/H_2O and UO_2/Ar scenarios followed a unique kinetic and were fitted using a simple Direct Impact model, but the kinetics were seen to depend on experimental conditions. During the UO_2 leaching study, the acquired data showed that irradiation defects are likely to be involved in chemical reactions occurring near the UO_2-H_2O interface. The UO_2 boundary acts as sinks and accelerate the annealing of defects. In regard to the UO_2/Ar system, it was reported that the elimination of defects solely depends on a simple interstitial-vacancy recombination mechanism. The latter was attributed to the chemically inert UO_2-Ar interface.

Finally, the irradiated water solution was analyzed to study the UO_2 oxidative dissolution mechanisms. It was observed that the concentration of radiolytic H_2O_2 and dissolved uranium were sufficient to allow the precipitation of secondary U(VI) phases in the form of studtite. In addition, the dissolution occurred without the formation of a UO_2 oxidized layer due to the combined effects of complexing fluoride ions and slightly acidic irradiated solution.

6. Acknowledgments

This work was conducted and funded within the framework of the French Tripartite Institute CEA/EDF/Framatome [Project Transport et Entreposage]. The authors are grateful to the EMIR committee and the technical staff of the CEMHTI facility. The authors also thank C. Tanguy and D. Drouan (CEA/DEN/LLCC) for their assistance with samples preparations and subsequent SEM analysis. Finally, J. Raynal and H. Rouquette (CEA/DEN/LCU) are warmly acknowledged for their contribution during XRD measurements.

7. Data availability

The raw/processed data that support the findings of this study are available from the corresponding author, [R. Mohun], upon reasonable request.

8. References

[1] D. Shoesmith and S. Sunder, *J. Nucl. Mater.* 190 (1992) 20-35. https://doi.org/10.1016/0022-3115(92)90072-S

[2] C. Corbel, G. Sattonnay, S. Guilbert, F. Garrido, M. Barthe and C. Jégou, *J. Nucl. Mater.* 348 (2006) 1-17. https://doi.org/10.1016/j.jnucmat.2005.05.009

[3] A. Poulesquen and C. Jégou, *Nucl. Tech.* 160 (2007) 337-345. https://doi.org/10.13182/NT07-A3904

[4] G. Sattonnay, C. Ardois, C. Corbel, J. Lucchini, M. Barthe, F. Garrido and D. Gosset, *J. Nucl. Mater.* 288 (2001) 11-19. https://doi.org/10.1016/S0022-3115(00)00714-5

[5] C. Jégou, B. Muzeau, V. Broudic, A. Poulesquen, D. Roudil, F. Jorion and C. Corbel, *Radiochim. Acta.* 93 (2009) 35–42. https://doi.org/10.1524/ract.93.1.35.58294

[6] G. Thomas and G. Till, *Nucl. Chem. Waste Management.* 5 (1984) 141-147. https://doi.org/10.1016/0191-815X(84)90044-5

[7] L. Johnsson, D. Shoesmith, G. Lunansky, M. Bailey and P. Termaine, *Nucl. Tech.* 56 (1982) 238-253. https://doi.org/10.13182/NT82-A32851

[8] M. Magnin, C. Jégou, R. Caraballo, V. Broudic, M. Tribet, S. Peuget and Z. Talip, *J. Nucl. Mater.* 462 (2015) 230-241. https://doi.org/10.1016/j.jnucmat.2015.03.029

[9] R. Forsyth and L. Werme, *J. Nucl. Mater.* 190 (1992) 3-19. https://doi.org/10.1016/0022-3115(92)90071-R

[10] V. Gromov, *Radiat. Phys. Chem.* 18 (1981) 135-146. https://doi.org/10.1016/0146-5724(81)90071-6

[11] F. Clarens, J. De Pablo, I. Diez-Pérez, I. Casas, J. Giménez and M. Rovira, *Environ. Sci. Technol.* 38 (2004) 6656-6661. https://doi.org/10.1021/es0492891

[12] S. Sunder, D. Shoesmith, H. Christensen, N. Miller and M. Bailey, *Mater. Res. Soc. Symp. Proc.* 176 (1989) 457. https://doi.org/10.1557/PROC-176-457

[13] S. Sunder, D. Shoesmith, H. Christensen and N. Miller, *J. Nucl. Mater.* 190 (1992) 78-86. https://doi.org/10.1016/0022-3115(92)90078-Y

[14] C. Jégou, B. Muzeau, V. Broudic, S. Peuget, A. Poulesquen, D. Roudil and C. Corbel, *J. Nucl. Mater.* 341 (2005) 62–82. https://doi.org/10.1016/j.jnucmat.2005.01.008

[15] P. Finn, J. Hoh, S. Wolf, S. Slater and J. Bates, *Radiochim. Acta.* 74 (1996) 65-71. https://doi.org/10.1524/ract.1996.74.special-issue.65

[16] J. Cobos, T. Wiss, T. Gouder and V. Rondinella, *Mater. Res. Soc. Symp. Proc.* 757 (2002) II9.2. https://doi.org/10.1557/PROC-757-II9.2

[17] W. Weber, R. Ewing, C. Catlow, T. Diaz de la Rubia, L. Hobbs, C. Kinoshita, H. Matzke, A. Motta, M. Nastasi, E. Salje, E. Vance and S. Zinkle, *J. Mater. Res.* 13 (1998) 1434-1484. https://doi.org/10.1557/JMR.1998.0205

[18] W. Weber and F. Roberts, *Nucl. Tech.* 60 (1983) 178-198. https://doi.org/10.13182/NT83-A33073

[19] C. Corkhill, D. Bailey, F. Tocino, M. Stennett, J. Miller, J. Provis, K. Travis and N. Hyatt, *ACS Appl. Mater. Interfaces*. 8 (2016) 10562–10571. https://doi.org/10.1021/acsami.5b11323

[20] D. Horlait, N. Clavier, S. Szenknect, N. Dacheux and V. Dubois, *Inorg. Chem.* 51 (2012) 3868-3878. https://doi.org/10.1021/ic300071c

[21] A. Popel, S. Le Solliec, G. Lampronti, J. Day, P. Petrov and I. Farnan, *J. Nucl. Mater.* 484 (2017) 332–338. https://doi.org/10.1016/j.jnucmat.2016.10.046

[22] K. Ollila, *Mater. Res. Soc. Symp. Proc.*127 (1988) 337. https://doi.org/10.1557/PROC-127-337

[23] H. Matzke, *J. Nucl. Mater.* 190 (1992) 101-106. https://doi.org/10.1016/0022-3115(92)90080-5

[24] M. Amme, B. Renker, B. Schmid, M. Feth, H. Bertagnolli and W. Dobelin, *J. Nucl. Mater.* 306 (2002) 202-212. https://doi.org/10.1016/S0022-3115(02)01291-6

[25] C. Jégou, R. Caraballo, S. Peuget, D. Roudil, L. Desgranges and M. Magnin, *J. Nucl. Mater*. 405 (2010) 235–243. https://doi.org/10.1016/j.jnucmat.2010.08.005

[26] G. Guimbretière, L. Desgranges, A. Canizarès, G. Carlot, R. Caraballo, C. Jégou, F. Duval, N. Raimboux, M. Ammar and P. Simon, *Appl. Phys. Lett.* 100 (2012) 251914. https://doi.org/10.1063/1.4729588

[27] M. Naji, J. Colle, O. Beneš, M. Sierig, J. Rautio, P. Lajarge and D. Manara, *J. Raman Spectrosc.* 46 (2015) 750–756. https://doi.org/10.1002/jrs.4716

[28] C. Jégou, M. Gennisson, S. Peuget, L. Desgranges, G. Guimbretière, M. Magnin, Z. Talip and P. Simon, *J. Nucl. Mater*. 458 (2015) 343–349. https://doi.org/10.1016/j.jnucmat.2014.12.072

[29] Ziegler J.F., *SRIM Software 2011*. Available online: http://www.srim.org

[30] A. Canizarès, G. Guimbretière, Y. Tobon, N. Raimboux, R. Omnée, M. Perdicakis, B. Muzeau, E. Leoni, M. Alam, E. Mendes, D. Simon, G. Matzen, C. Corbel, M. Barthe and P. Simon, *J. Raman Spectrosc.* 43 (2012) 1492-1497. https://doi.org/10.1002/jrs.4088

[31] S. Le Caër, *Water*. 3 (2011) 235-253. https://doi.org/10.3390/w3010235

[32] J. Spinks and R. Woods, An Introduction to Radiation Chemistry, 3rd ed., New York, USA: Wiley-Interscience publication, 1991. https://doi.org/10.1002/bbpc.19910950346

[33] G. Guimbretière, L. Desgranges, A. Canizarès, R. Caraballo, F. Duval, N. Raimboux, R. Omnée, M. Ammar, C. Jégou and P. Simon, *Appl. Phys. Lett.*103 (2013) 041904. https://doi.org/10.1063/1.4816285

[34] G. Hochanadel, *J. Phys. Chem.* 56 (1952) 587-594. https://doi.org/10.1021/j150497a008

[35] G. Guimbretière, A. Canizarès, N. Raimboux, J. Joseph, P. Desgardin, L. Desgranges, C. Jégou and P. Simon, *J. Raman Spectrosc.* 46 (2015) 418-420. https://doi.org/10.1002/jrs.4661

[36] L. Desgranges, G. Guimbretière, P. Simon, F. Duval, A. Canizarès, R. Omnée, C. Jégou and R. Caraballo, *Nucl. Instrum. Methods B.* 327 (2014) 74–77. https://doi.org/10.1016/j.nimb.2013.10.083

[37] T. Livneh and E. Sterer, *Phys. Rev. B.* 73 (2006) 085118. https://doi.org/10.1103/PhysRevB.73.085118

[38] Z. Talip, T. Wiss, P. Raison, J. Paillier, D. Manara, J. Somers and R. Konings, *J. Am. Ceram. Soc.* 98 (2015) 2278–2285. https://doi.org/10.1111/jace.13559

[39] R. Mohun, L. Desgranges, J. Léchelle, G. Guimbretière, P. Simon, A. Canizarès, F. Duval, C. Jégou, M. Magnin, N. Dacheux, N. Clavier, C. Valot and R. Vauchy, *Nucl. Instrum. Methods B.* 374 (2016) 67-70. https://doi.org/10.1016/j.nimb.2015.08.003

[40] A. Traboulsi, J. Vandenborre, G. Blain, B. Humbert, F. Haddad and M. Fattahi, *J. Nucl. Mat.* 467 (2015) 832-839. https://doi.org/10.1016/j.jnucmat.2015.10.061

[41] K. Walenta, *American Mineralogist.* 59 (1974) 166-171.

[42] D. Shoesmith and S. Sunder, 1991. [Online]. http://www.iaea.org/inis/collection/NCLCollectionStore/_Public/23/078/23078146.pdf [Accessed 25 July 2017].

[43] H. Kubatko, K. Helean, A. Navrotsky and P. Burns, *Science.* 302 (2003) 1191-1193. https://doi.org/10.1126/science.1090259

[44] M. Torrero, E. Baraj, J. De Pablo, J. Giménez and I. Casas, Int. J. Chem. Kinet. 29 (1997) 261-267. https://doi.org/10.1002/(SICI)1097-4601(1997)29:4<261::AID-KIN4>3.0.CO;2-S

[45] D. Manara and B. Renker, *J. Nucl. Mater.* 321 (2003) 233-237. https://doi.org/10.1016/S0022-3115(03)00248-4

[46] H. He and D. Shoesmith, *Phys. Chem. Chem. Phys.* 12 (2010) 8109-8118. https://doi.org/10.1039/B925495A

[47] L. Desgranges, G. Baldinozzi, P. Simon, G. Guimbretière and A. Canizarès, *J. Raman Spectrosc.* 43 (2012) 455-458. https://doi.org/10.1002/jrs.3054

[48] J. Elorrieta, L. Bonales, N. Rodriguez-Villagra, V. Baonza and J. Cobos, *Phys. Chem. Chem. Phys.*18 (2016) 28209-28216. https://doi.org/10.1039/C6CP03800J

[49] R. Böhler, A. Quaini, L. Capriotti, P. Cakir, O. Benes, K. Boboridis, A. Guiot, L. Luzzi, R. Konings and D. Manara, *J. Alloys Comp.* 616 (2014) 5-13. https://doi.org/10.1016/j.jallcom.2014.07.055

[50] W. Weber, *J. Nucl. Mater.* 98 (1981) 206–215. https://doi.org/10.1016/0022-3115(81)90400-1

[51] F. Tocino, S. Szenknect, A. Mesbah, N. Clavier and N. Dacheux, *Prog. Nucl. Energy.* 72 (2014) 101-106. https://doi.org/10.1016/j.pnucene.2013.09.014